

Article

Flood Risk Assessment Based on Hydrodynamic Model—A Case of the China–Pakistan Economic Corridor

Xiaolin Sun ¹, Ke Jin ¹, Hui Tao ², Zheng Duan ³ and Chao Gao ^{1,4,*} 

¹ Department of Geography and Spatial Information Techniques, Zhejiang Collaborative Innovation Center & Ningbo Universities Collaborative Innovation Center for Land and Marine Spatial Utilization and Governance Research, Ningbo University, Ningbo 315211, China; sss093098@163.com (X.S.); jinke505320@163.com (K.J.)

² State Key Laboratory of Desert and Oasis Ecology, Xinjiang Institute of Ecology and Geography, Chinese Academy of Sciences, Urumqi 830011, China; happyzjh0628@gmail.com

³ Department of Physical Geography and Ecosystem Science, Lund University, 223 62 Lund, Sweden; huangfujue3@gmail.com

⁴ Donghai Academy, Zhejiang Ocean Development Think Tank Alliance, Ningbo University, Ningbo 315211, China

* Correspondence: gaoqinchao1@163.com

Abstract: Under global warming, flooding has become one of the most destructive natural disasters along the China–Pakistan Economic Corridor (CPEC), which significantly jeopardizes the construction and ongoing stability of the CPEC. The assessment of regional flood potential is, therefore, crucial for effective flood prevention and relief measures. In light of this, our study applied MIKE 11 hydrodynamic model for the Indus River Basin of Pakistan to achieve a comprehensive analysis of the flood-affected locations and depths under typical scenarios. The flood risk zones along the CPEC were evaluated using the indicator system method in conjunction with the combination weighting method. The results show that the hydrodynamic model has a Nash–Sutcliffe efficiency of 0.86, allowing for the investigation of floods at more precise temporal and spatial scales. Punjab, Sindh, and Balochistan Provinces are the main inundation areas under a 100-year flood scenario, with inundation depths ranging from 1 to 4 m. The coastal regions of Sindh and Hafizabad in Punjab witnessed the most severe floods, with maximum inundation depths exceeding 8 m. Flooding predominantly impacts the southeastern region of the CPEC. The medium- to high-risk zones comprise 25.56% of the region, while high-risk areas constitute 4.18%. Particularly, the eastern and southern regions of Punjab, along with the central and southern regions of Sindh, have been pinpointed as high-risk areas, primarily due to their dense population and riverine characteristics. Overall, our findings provide a scientific basis for informed decision making pertaining to disaster reduction and flood prevention.

Keywords: CPEC; flood risk assessment; hydrodynamic model; analytic hierarchy process; entropy weight method



Citation: Sun, X.; Jin, K.; Tao, H.; Duan, Z.; Gao, C. Flood Risk Assessment Based on Hydrodynamic Model—A Case of the China–Pakistan Economic Corridor. *Water* **2023**, *15*, 4295. <https://doi.org/10.3390/w15244295>

Academic Editor: Athanasios Loukas

Received: 19 October 2023

Revised: 9 December 2023

Accepted: 12 December 2023

Published: 16 December 2023



Copyright: © 2023 by the authors. Licensee MDPI, Basel, Switzerland. This article is an open access article distributed under the terms and conditions of the Creative Commons Attribution (CC BY) license (<https://creativecommons.org/licenses/by/4.0/>).

1. Introduction

It is an accepted fact that climate change is characterized by rising temperatures globally [1]. This warming intensifies the water cycle, significantly increasing the likelihood of extreme precipitation and flooding events. According to statistics, between 1995 and 2015, over 2.2 billion people were affected by floods, comprising 53% of the total of people affected by all weather-related disasters [2], making them one of the most prevalent, widespread, and socioeconomically devastating natural disasters [3]. This highlights the urgent need for robust, scientifically sound disaster risk management strategies. Quantitative flood risk assessment is a crucial prerequisite for effective risk management and minimizing flood damage, especially as climate extremes become more frequent. Current flood risk assessment methods can be categorized into three main approaches: indicator system method, historical disaster statistics, and scenario simulation modeling. The indicator system method is primarily based on the characteristics of the research area. It

involves selecting evaluation indicators at each level and determining their respective weights, subsequently obtaining the corresponding index of regional flood risk [4,5]. For instance, Peng and Zhang (2022) quantified flood risks in Zhengzhou using an indicator system reflecting natural and social vulnerabilities [6]. Historical disaster statistics utilize mathematical and theoretical techniques to analyze past flood patterns and extrapolate future hazard likelihoods [7,8]. Benito et al. (2004) assessed flood frequency in Europe using long-term hydrologic data series to establish a fundamental basis for more precise flood risk assessment [9]. The scenario simulation modeling involves generating flood inundation zones through simulating water movement in flood-prone areas [10], enabling the evaluation of flood risk under diverse scenarios. One of the more prevalent methods involves simulating and analyzing flood scenarios by using hydrodynamic models. For example, Taraky et al. (2021) utilized the SWAT hydrological model to forecast peak flood flows and subsequently simulated the inundation characteristics of the Kabul River Basin [11].

Flood risk is generally defined as the combined representation of hazard, vulnerability and exposure [12]. Nevertheless, individually applying indicator, historical, or simulation methods makes adequately capturing the complex interrelationships and dynamics within flood systems challenging. The indicator system method comprehensively takes into account the flood hazards and the socioeconomic characteristics, but the selection of indicators of the disaster-causing factors is mostly based on the historical rainfall/flow data, which cannot accurately reflect the water accumulation on the ground and ignore the process of flood production. The historical disaster method uses historical information to calculate flood frequency, but the use of the historical disaster method is very dependent on specimen data and is not applicable in information-poor regions. The scenario simulation assessment method takes into account the flood formation process compared to the previous two methods, but it fails to articulate and calculate the socioeconomic impact of floods. With the development of hydrodynamic models, the flood risk assessments combining the indicator method and the scenario simulation method has received increasing research attention. This integrated approach considers the evolution of floods by using a model, the socioeconomic impacts of floods by using an indicator system and the typicality of floods by using historical data. The integrated approach has become a new assessment method that takes full account of flood risk because of its comprehensive advantages. For example, Zhao et al. (2022) used Info Works ICM to simulate urban waterlogging scenarios with different recurrence intervals and evaluate the risk of waterlogging disasters in Tianhe District of Guangzhou [13]. Zhang et al. (2023) employed a hydrodynamic model to simulate extreme flooding in a coastal city and assessed the effects of natural and anthropogenic drivers on extreme flood events in coastal regions [14]. However, it is currently applied more in urban areas, which are characterized by small basin areas, small river drops, short river confluence time and short river flow. The present research is not representative of the areas with large basin areas, large river drops, long confluence time and large river discharge. Therefore, it is necessary to carry out work in basin-wide flood risk assessment and prevention.

The China–Pakistan Economic Corridor (CPEC) is situated in the South Asian subcontinent, with the Indus River serving as the international waterway that traverses through the corridor. The Indus River Basin in the CPEC covers an area of about 561,000 km², with the highest point of the basin being 8569 m and the lowest point being −44 m. It also has a large drop, and the river flow and the confluence time are long. Therefore, we adopt an integrated approach to flood risk assessment in the Indus River Basin. This study can not only improve the reliability and directness of flood risk assessment results but also provide some reference for large-scale and basin-wide flood risk assessment. The increase in both the frequency and intensity of flooding is attributed to the surge in extreme precipitation within the region. Pakistan experienced severe flooding and significant social and economic damage during the summer of 2022 due to rainfall that exceeded the annual average by 87%. However, current research on flood risk within the CPEC [15–20] has focused on spatiotemporal changes in floods, causes of flooding, and simulations of snowmelt floods,

but comprehensive flood risk assessment remains limited. There is an urgent need to enhance flood modeling and risk assessment across the CPEC region.

Our study aimed to simulate flood evolution in the CPEC region under typical scenarios using the MIKE 11 hydrodynamic model. The simulation results were visualized on a map utilizing the ArcGIS 10.5 software. Additionally, we developed an integrated risk assessment framework encompassing flood hazard, sensitivity, and vulnerability indicators, with weights assigned through the Analytic Hierarchy Process and Entropy Weight Method. Our results are expected to establish a foundation for implementing disaster prevention and ensuring uninterrupted connectivity along the CPEC.

2. Materials and Methods

2.1. Study Area

The CPEC (Figure 1) is a significant corridor that establishes a connection between Kashgar in Xinjiang, China, and the port of Gwadar in southwest Pakistan. Its route passes through all of Pakistan's provinces, as well as Kashgar in Xinjiang, China, and its surrounding regions. The corridor spans a total length of approximately 3000 km and covers an extensive area measuring around 927,597 km². The main tributaries of the Indus River, namely, the Jhelum, Chenab, Ravi, and Sutlej Rivers converge at the Punjab Plain, where river flow is slowed by topography, and riverbeds rise steadily as a result of accumulating sediments, leading to the formation of suspended rivers. Furthermore, problems such as insufficient water discharge capacity and poor flood prevention measures for dams within the basin are prominent due to the peculiarities of the Pakistani situation [21].

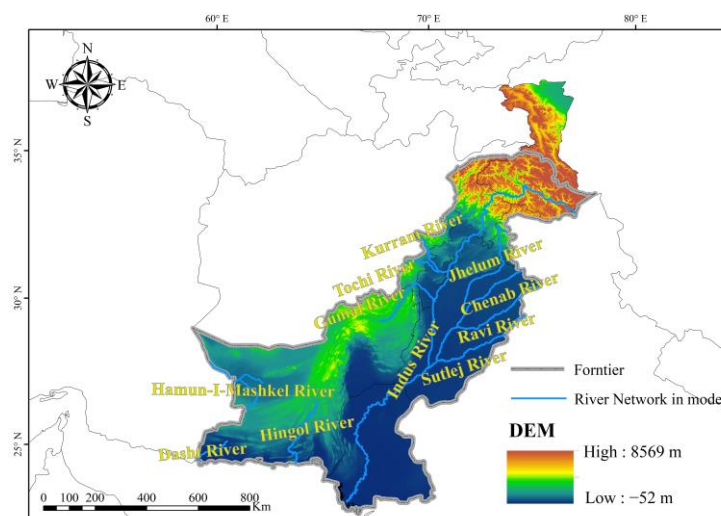


Figure 1. Sketch map of the China-Pakistan Economic Corridor.

Pakistan's southern border with the Arabian Sea. The topography is generally high in the west and north, and low in the east and south. The Indus River runs through the country from north to south. During an active South Asian monsoon or a more favorable tropical disturbance in the Indian Ocean, strong southerly winds carry abundant moisture deep into the interior of Pakistan and produce heavy precipitation on the windward slopes of the mountains [22]. The heavy precipitation rushes into the Indus, causing the river to surge upstream and pour down along the high north and low south terrain, making it highly susceptible to flooding in the middle and lower reaches of the Indus. Consequently, this phenomenon has contributed to elevated water levels in the upper Indus River, thereby amplifying the risk of flooding in densely populated regions located along the middle and lower reaches. Severe casualties and socioeconomic damage from recent floods [23] underscore the need for comprehensive catastrophe risk assessments in the CPEC.

2.2. Hydrodynamic Model

In the flood modeling process, the main emphasis of the 1D model is on the confluence process of the river, while the 2D model emphasizes the spatial impact of the flood. Since 1D models require less input data than 2D models, they are easier to set up and calibrate [24]. It is generally acknowledged that 1D model results are robust when the main flow occurs along the direction of the main river channel [25]. In contrast, although the increase in computing power has multiplied the use of 2D, they are still limited to smaller spatial-scale studies [26–28]. As compared to 1D models, 2D models permit a more accurate simulation of flow processes. However, for practical applications where large, flooded areas are to be involved, 2D or even 3D models do not necessarily perform better [26,27]. Consequently, although more complex approaches exist, when dealing with simulation of flood events, the use of 1D models is still common. The 1D models are especially true for cases where steady-state conditions of flows are considered [29].

From the current study, 2D models are mainly used for refined simulation of small areas. This is because if the 2D model is applied to a large area, it may be computationally unstable, leading to inaccurate model simulation results. In addition to this, due to objective constraints, we do not have rich access to the type of data available for the Pakistani region, which also contributes to some extent to the difficulty in applying 2D models. The 1D model is more applicable for flood simulation in the Indus Basin.

In addition, there is undeniable presence of wide valleys in the region of the CPEC. The valley area is located in the upper Indus River. It accounts for no more than 35% of the area, which has a relatively small impact on the model as a whole. In summary, the MIKE11HD model was selected for flood evolution simulation in the CPEC region based on the performance and application scope of the model.

We constructed the MIKE11HD model by first screening for the river class. The major tributaries of the Indus, such as the Jhelum and Ravi Rivers, as well as the main stream of the Indus, have been selected for the construction of the river network of the basin. Subsequently, we selected channel cross-section data with wider cross sections for input into the model. Even in the event of flood inundation, the wider channel cross section ensures that the inundated area is within the channel cross section, mitigating the adverse effects of complex terrain, such as valleys, on the modeling results. We also used the start of each river as the upper boundary of the model and the point where the Indus enters the sea as the lower boundary, and we entered the corresponding hydrological information to complete the setting of the basin boundary. Finally, parameters such as roughness were assigned, and after rate determination and validation, suitable parameter information was selected to complete the construction of the flood evolution model for the Indus River Basin.

The MIKE 11HD [30] model is one of the most widely used hydrodynamic models. Developed by the Danish Hydraulic Institute, it provides a robust simulation platform that accurately predicts water surface profiles and river discharge. By using a six-point Abbott–Ionescu finite difference format to solve the St. Venant Equation (1), this model effectively estimates water levels and flow velocities at alternating sites along the river network with utmost precision and efficiency. With its exceptional computational capabilities and reliable performance over extended temporal and spatial scales, the MIKE 11 HD proves particularly well suited for analyzing intricate river networks within CPEC.

$$\begin{cases} B_s \frac{\delta Q}{\delta x} + \frac{\delta A}{\delta t} = q \\ \frac{\delta Q}{\delta t} + \frac{\delta \left(a \frac{Q^2}{A} \right)}{\delta x} + gA \frac{\delta h}{\delta x} + \frac{g|Q|Q}{C^2 AR} = 0 \end{cases} \quad (1)$$

where B_s is the water surface river width, m; Q is the flow rate (m^3/s); q is the lateral inflow (m^3/s); A is the overwater area (m^2); h is the water level, m; R is the hydraulic radius (m), C is the Xie Cai coefficient; a is the momentum correction factor; x , t are the spatial coordinates (m) and time coordinates (s); g is the gravitational acceleration (m/s^2).

2.3. Data

- (1) The geographic data, including the Digital Elevation Model (DEM) and derived slope data, were obtained from the Geographic Spatial Cloud (<http://www.gscloud.cn/>, accessed on 13 December 2023). These datasets were utilized for hydrological network extraction, stream and cross-section file creation, as well as terrain file production within the study area. The Normalized Difference Vegetation Index (NDVI) data for 2020 were acquired from NASA's regularly updated MOD13A3 dataset (<https://search.earthdata.nasa.gov/search>, accessed on 10 December 2023). NDVI data were resampled to a 90 m × 90 m resolution and normalized for further analysis.
- (2) The socioeconomic datasets include the population density in 2020 derived from the World Pop website (<https://www.worldpop.org/datacatalog/>, accessed on 3 December 2023). The 30 m annual land cover dataset was from the GlobeLand30 dataset, (<https://www.webmap.cn/>, accessed on 10 December 2023) and road data were acquired from the Socioeconomic Data and Applications Center (<https://sedac.ciesin.columbia.edu>, accessed on 9 December 2023). All these datasets were resampled to a 90 m × 90 m spatial resolution and normalized for further analysis.
- (3) Daily river discharge data from 2003 to 2010 were obtained from stations along the Indus, Chenab, Jhelum, Ravi, and Sutlej Rivers. Data for the Tarbela, Marala, Mangla, Balloki, and Ganda Singhwala stations were provided by the Pakistan Water and Power Development Authority (WAPDA). These data were critical for hydraulic model boundary and time series file generation, calibration, and validation. Additionally, satellite-derived estimates of daily discharge and water level data were acquired from the German Inland Waterway Hydrology Time Series Database (DAHITI, <https://dahiti.dgfi.tum.de/en/>, accessed on 7 December 2023) for downstream Indus River segments over 2003–2010. These supplementary hydrologic data were further employed in the calibration and validation processes of the modeling.

The files required to construct the MIKE11HD model are shown in Table 1. After preparing the files according to the above data, the simulation module of MIKE11HD inputs these files to complete the construction of the 1D flood evolution model.

Table 1. Documentation of the MIKE11HD.

Number	File Name	Source	Format	Type	Description	Website
1	River network	Extraction of river network using preprocessed DEM data of the CPEC	.nwk11	Line file	The rivers in the study area mainly include the Indus River, Jhelum River, Chenab River, etc.	http://www.gscloud.cn/ , accessed on 9 December 2023
2	Cross section	Cross section information provided by the Government of Pakistan, Cross section information extracted from preprocessed DEM and remote sensing images	.xns11	Electronic document	Cross section information on major rivers in the Indus basin	/
3	Boundary condition	Discharge information from hydrological stations provided by the Government of Pakistan, Water level information obtained from the DAHITI	.dfs0	Electronic document	Hydrological data of major rivers in the Indus Basin	https://dahiti.dgfi.tum.de/en/ , accessed on 9 December 2023

2.4. Flood Hazard Risk Assessment Methods

When conducting flood risk assessments, it is crucial to accurately determine the appropriate weights based on the contribution of different variables. Subjective and objective weighting techniques are two widely used methods for indicators [31]. However, each has its limitations when applied in isolation. Therefore, thoughtfully integrating multiple weighting approaches is important to balance decision maker priorities and real-world conditions. This study combines AHP, entropy weighting, and the minimal relative entropy principle to leverage their complementary strengths. The AHP incorporates expert opinions on indicator importance. The entropy weighting objectively assigns weights based on the underlying data structure. The minimal relative entropy principle then integrates the two sets of weights with maximum preservation of original information. This multifaceted weighting framework allows for a more objective, balanced, and acceptable flood risk assessment model formulation.

2.4.1. AHP Method

The AHP hierarchical analysis is a multi-level weighting technique that incorporates expert judgments into the analytical process. It involves hierarchical structures, such as target layer–criteria layer–indicator layer, constructing a two-by-two judgment matrix, which compares the relative importance of elements within each hierarchy, quantifying these comparisons to determine the subjective weights w'_j for each indicator, and conducting consistent analysis (2). A consistency ratio (CR) below 0.1 indicates a reasonable overall ranking of the hierarchy, while a CR above 0.1 suggests an unreasonable ranking requiring reconstruction and retesting of matrices for consistency.

$$\begin{cases} CI = \frac{\lambda_{max} - m}{m - 1} \\ CR = \frac{CI}{RI} \end{cases} \quad (2)$$

where λ_{max} is the maximum eigenvalue of the judgment matrix, m is the order of the judgment matrix, RI is the average random consistency index, and the value of RI corresponding to the judgment matrix can be obtained by consulting the table [32].

2.4.2. Entropy Weight Method

The entropy weighting method objectively assigns weights to indicators based on the degree of variability in the underlying data. It utilizes information entropy to calculate an entropy weight for each indicator, which is then used to adjust the weight to be more objective. The specific steps are: The data of each positive (P) and negative (N) indicator (3) will be normalized to construct the indicator matrix Y_{ij} :

$$\begin{cases} y_{ij} = \frac{x_{ij} - \min x_{ij}}{\max x_{ij} - \min x_{ij}} (P) \\ y_{ij} = \frac{\max x_{ij} - x_{ij}}{\max x_{ij} - \min x_{ij}} (N) \end{cases} \quad (3)$$

To measure entropy, the entries of matrix Y_{ij} are represented in a probability distribution, P_{ij} . The probability value (P_{ij}) for each entry in the matrix is determined by normalizing criteria performance values at each decision alternative. Using the normalized values from (4), the P_{ij} matrix will be formed:

$$P_{ij} = \frac{Y_{ij}}{\sum_{i=1}^m Y_{ij}} \quad (4)$$

The entropy e_j for a set of outcomes (n decision alternatives) at a decision criterion j is defined as:

$$e_j = -k \sum_{i=1}^m P_{ij} \ln P_{ij} \quad (5)$$

$k = \frac{1}{\ln m}$, where m is the number of pixels in the indicator study area, i.e., the nine regions of the CPEC.

The degree of diversification g_j of the information provided by a decision criterion j is defined as:

$$g_j = 1 - e_j \quad (6)$$

An attribute in which all alternatives have similar values has little discriminatory power (small g_j values) and thus should be given less weight. The objective criteria weight set w_j'' can be defined as follows:

$$w_j'' = \frac{g_j}{\sum_{j=1}^n g_j} \quad (7)$$

where n is the number of tertiary indicators.

2.4.3. Combined Weight

By incorporating the subjective influence of the AHP hierarchical analysis method and the objective impact of the entropy weighting method, the limitations inherent in both approaches can be overcome through the adoption of the minimum relative entropy method for determining the combined weights [33]. The final set of criteria weights (w_j) is derived by integrating both objective and subjective weights using the Lagrange method as follows:

$$w_j = \sqrt{w_j' w_j''} / \sum_{j=1}^m \sqrt{w_j' w_j''} \quad (8)$$

2.5. Hydrodynamic Model Simulation

2.5.1. Data Used in the MIKE11HD Model

The key data requirements for the MIKE 11HD model include topography, river geometry, and hydrologic time series. The Indus River Basin digital river network was derived from CPEC regional DEM data using Arc GIS Spatial Analyst tools. The MIKE11HD River Network tool then generated the model river network file.

Accurate cross-section data defining river geometry are critical for model stability. Cross sections were inserted at key river locations based on satellite imagery and DEM analysis. Specifically, 32 cross sections were obtained for the Jhelum River, 43 for the Chenab, 22 for the Ravi, 15 for the Sutlej, and 145 for the Indus. To accurately simulate scenarios, appropriate boundary conditions are needed. Upstream boundaries utilized daily 2003–2010 discharge data from the Tarbela, Marala, Mangla, Balloki, and Ganda Singhwala stations. The downstream boundary employed daily water level data over the same period from station 6830 from DAHITI. Initial conditions were set to 1 m water level and 0.2 m³/s discharge to prevent dry riverbed simulation and match real initial hydraulics within the river network. Unlike other hydrological models, the calibration process for the MIKE 11HD model requires fewer datasets. Instead, appropriate model parameters and input boundary conditions were established to represent the physical process of river flow. For calibration, daily water level data from 2003 to 2007 from station 10220 in the DAHITI were used. The calibrated model was then validated with water level data from 2007 to 2010 from the same DAHITI station.

2.5.2. Calibration and Validation of the MIKE11 Model

The river channel roughness coefficient (Manning's n) is a critical calibration parameter impacting model performance. Manning's n values were iteratively adjusted until simulated water levels closely matched observations. To evaluate the accuracy of the model, widely used metrics, including Nash–Sutcliffe efficiency coefficient (E_{ns}), the coefficient of determination (R^2), and the root-mean-square error ($RMSE$), were used. Their formulas are as follows:

(1) Nash–Sutcliffe efficiency coefficient (E_{ns}):

The Nash–Sutcliffe efficiency coefficient is generally used to verify the quality of hydrological model simulation results. The E_{ns} value can range from $-\infty$ to 1. The E_{ns} value of 1 reflects a perfect match between the measured and modeled values. If the E_{ns} value is less than zero, the measured mean is a better predictor than the model. If the E_{ns} value is equal to zero, the modeled values are as accurate as the mean of the measured data.

The formula for calculating E_{ns} is as follows:

$$E_{ns} = 1 - \frac{\sum_{i=1}^n (Q_m - Q_p)^2}{\sum_{i=1}^n (Q_m - Q_a)^2} \tag{9}$$

where n is the number of data pairs, Q_m is the measured data value, Q_p is the simulated value, and Q_a is the average measured value.

(2) Coefficient of determination (R^2):

The coefficient of determination is an indicator that evaluates the degree of agreement between predicted and actual values. The closer R^2 is to 1, the greater the correlation. Conversely, the closer R^2 is to 0, the smaller the correlation. The formula for calculating R^2 is as follows:

$$R^2 = \frac{[\sum_{i=1}^n (S_i - \bar{S})(M_i - \bar{M})]}{\sum_{i=1}^n (S_i - \bar{S})^2 \sum_{i=1}^n (M_i - \bar{M})^2} \tag{10}$$

where S_i is the measured data, \bar{S} is the average of the measured data, M_i is the simulated value, and \bar{M} is the average of the simulated value.

(3) Root-mean-square error ($RMSE$):

The $RMSE$ ranges from 0 to ∞ . At an ideal fit, the $RMSE$ is equal to zero. The $RMSE$ values are widely used to compare the errors of models as compared to the measured data. The formula for calculating $RMSE$ is as follows:

$$RMSE = \sqrt{\frac{1}{n} \sum_{i=1}^n (y_i - \hat{y}_i)^2} \tag{11}$$

where y_i is the measured value, \hat{y}_i is the simulated value, and n is the number of data pairs.

3. Results

3.1. The MIKE11HD Model

The MIKE 11HD model was calibrated by changing the values of Manning’s roughness coefficients (n) in the river reach. During calibration, the simulated water levels and the observed water levels at station 10220 in the DAHITI were compared for different combinations of n till the simulated and observed water levels matched closely. According to hydraulic manuals, the Manning’s roughness coefficient for the Indus River Basin should be between 0.015 and 0.035, as it is mostly composed of natural sandy riverbeds. In this work, the roughness coefficient was initially set to 0.025.

In general, simulation of the model is considered reasonable when $E_{ns} \geq 0.5$, $R^2 \geq 0.6$ and the closer the $RMSE$ is to about 0. By comparing the parameter calibration results of the model in Table 2, we can observe that the model performs well when the riverbed roughness is set to 0.02, E_{ns} value is 0.724, R^2 is 0.719 and the $RMSE$ is 0.495.

Table 2. Results of riverbed roughness measurement.

Roughness	0.015	0.020	0.025	0.030	0.035
E_{ns}	0.639	0.724	0.440	−0.135	−0.916
R^2	0.734	0.739	0.745	0.750	0.753
$RMSE$	0.500	0.495	0.490	0.485	0.481

Based on water level data during the corresponding time period at station 10220, the validation results are shown in Table 3 and Figure 2. The Nash–Sutcliffe efficiency (E_{ns}) is 0.861, and the coefficient of determination (R^2) is 0.864, and the RMSE is 0.403, indicating that selecting a roughness value of 0.02 for the river is reasonable.

Table 3. Results of riverbed roughness verification.

Roughness	0.020
E_{ns}	0.861
R^2	0.864
RMSE	0.403

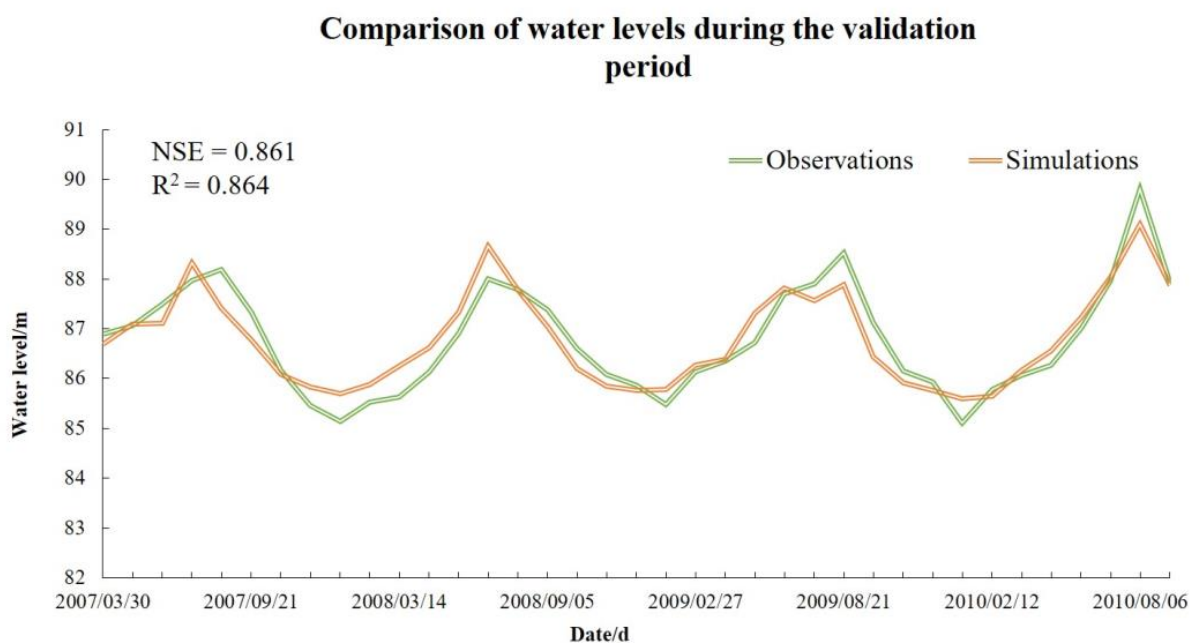


Figure 2. Comparison of observed and simulated water levels in validation period.

3.2. Flood Disaster Risk Assessment System

3.2.1. Determination of Flood Hazard Risk Assessment Indicators

Flood hazard arises from complex interactions between disaster-triggering factors, vulnerable receptors, and the physical environment. Therefore, indicator selection for risk assessment should integrate qualitative and quantitative data tailored to local conditions. Inundation depth is a key indicator due to its direct relationship with flooding likelihood.

As transportation infrastructure is vital for CPEC operations and agriculture crucial to Pakistan's economy, indicators should capture flood impacts on populations, infrastructure, and livelihoods. Considering the impact of floods on population, transportation, and agriculture, positive indicators, such as population density, arable land density, and road density, were chosen as measures for disaster-bearing capacity. Flood redistribution is affected by the natural conditions of the underlying surface [34]. Therefore, negative indicators, such as elevation, slope, and NDVI, were selected as indicators of a disaster-forming environment for flood risk assessment. To sum up, assessment indicators were developed by considering the danger posed by disaster-causing factors, the vulnerability of a disaster-bearing body, and the sensitivity of a disaster-forming environment (Table 4).

Table 4. Index system of flood disaster risk assessment.

Goal Level	Criterion Level	Indicator Level	Indicator Property
Flood disaster risk assessment of CPEC	Hazardousness of Hazard	flooding depth	P
	Vulnerability of Exposure	population density	P
		road density	P
		cultivated land density	P
	Sensitivity of Environment to Disasters	DEM	N
		slope	N
NDVI		N	

3.2.2. The Calculation of Weights for Flood Risk Assessment Indicators

Since indicators contribute differently to overall flood risk, both subjective and objective methods were used to determine weights.

(1) Analytic Hierarchy Process (AHP)

AHP matrices were constructed for the target, criteria, and indicator layers of the flood risk assessment framework. Pairwise comparisons between elements at each layer were scored using a 1–9 scale based on expert judgments.

The target layer is flood risk in this paper, the criteria layers are causative factor, disaster-prone environment and carrier system, the indicator layer is made up of representative elements from each of the criterion layers. First, we create the discriminant matrix (Table 5) between the criterion layer and the target layer. From this, we can observe that the disaster-prone environment has the highest weight, followed by the causative factor in second place, and the carrier system has the lowest weight.

Table 5. Weight allocation of judgment matrix between the goal level and criterion level.

Flood Risk	Carrier System	Disaster-Prone Environment	Causative Factor	Weight
Carrier system	1	0.5	0.5	0.196
Disaster-prone environment	2	1	2	0.493
Causative factor	2	0.5	1	0.311

Note: Where $\lambda = 3.0536$ CR = 0.0516 < 0.1 CI = 0.027.

Secondly, the judgment matrices of the indicator layer relative to the guideline layer were established (Tables 6 and 7), from which it can be seen that population density is the dominant indicator leading to the vulnerability of the carrier system, whereas the sensitivity in the disaster-prone environment is mainly influenced by elevation.

Table 6. Weight allocation of the hazard level of the indicator layer–causal factor matrix.

Carrier System	Population Density	Road Density	Cultivated Land Density	Weight
population density	1	2	3	0.540
road density	0.5	1	2	0.297
cultivated land density	0.333	0.5	1	0.163

Note: Where $\lambda = 3.0092$ CR = 0.0088 < 0.1 CI = 0.005.

Table 7. Weight allocation of the index layer-to-hazard factor risk assessment matrix.

Disaster-Prone Environment	Slope	NDVI	DEM	Weight
slope	1	3	0.333	0.250
NDVI	0.333	1	0.167	0.095
DEM	3	6	1	0.655

Note: Where $\lambda = 3.0183$ CR = 0.0176 < 0.1 CI = 0.009.

The consistency ratio (CR) of all the comparison matrices was less than 0.1, indicating reasonable consistency in the expert judgments. This suggests appropriate preliminary weighting of the indicators for risk assessment analysis. The weights across criteria and indicator layers were synthesized to derive the final AHP weights for each indicator, as shown in Table 8.

Table 8. The weights of each indicator in the Analytic Hierarchy Process (AHP).

Goal	Weight	Index	Weight
Hazard	0.311	flooding depth	0.311
		population density	0.106
Vulnerability	0.196	road density	0.058
		cultivated land density	0.032
		DEM	0.323
Sensitivity	0.493	slope	0.123
		NDVI	0.047

(2) Entropy Weight Method

Due to the evaluation unit being a 90 m × 90 m grid, the subareas of the CPEC were chosen as the fundamental evaluation objects in order to mitigate excessive computational complexity. Data for seven indicators were present within each evaluation object, which were normalized and employed to calculate the mean value of each indicator for that specific evaluation object. Consequently, a 9 × 7 evaluation indicator matrix was constructed and subsequently used to determine the weights. The results are shown in Table 9.

Table 9. The weights of each indicator using the Entropy Method.

Goal	Weight	Index	Weight
Hazard	0.429	flooding depth	0.429
		population density	0.229
Vulnerability	0.418	road density	0.098
		cultivated land density	0.092
		DEM	0.052
Sensitivity	0.153	slope	0.056
		NDVI	0.045

(3) Integrated Weighting

The subjective AHP weights and objective entropy weights were integrated using the minimum relative entropy principle to determine the final combined weights for risk assessment. As shown in Table 10, this produced balanced weights reflecting both expert opinions and data structure. It is evident from the table that the hazard has the highest weight, followed by vulnerability, and sensitivity has the smallest weight. Additionally, flood depth is identified as the primary factor influencing flood risk.

Table 10. Combination weight.

Goal	Index	Combination Weight	Analytic Hierarchy Process Weight	Entropy Weight	Combination Weight
Hazard	flooding depth	0.402	0.311	0.429	0.402
Vulnerability	population density	0.314	0.106	0.229	0.171
	road density		0.058	0.098	0.083
	cultivated land density		0.032	0.092	0.060
Sensitivity	DEM	0.284	0.323	0.052	0.142
	slope		0.123	0.056	0.091
	NDVI		0.047	0.045	0.051

3.3. Flood Hazard Assessment

3.3.1. Processing of Flood Hazard Indicators

The Pakistani government has undertaken extensive renovations on several river barrages, including the Guddu, Sukkur, and Kotri barrages, with the aim of enhancing flood control capabilities within the Indus River Basin. As a result, the region's flood protection requirements have been bolstered to withstand a 100-year return period. Furthermore, it can be concluded from the Pakistan Water and Power Development Authority's annual flood reports that catastrophic floods experienced between late July and early August in 2010 were nearly unprecedented in magnitude, comparable to events occurring once every century. Leveraging available flood data and information, this specific time frame has been chosen as a representative scenario for conducting a comprehensive flood inundation analysis.

Based on the simulation results obtained from the MIKE11HD model, the flood progression of each river during the period of 27–30 July 2010 was analyzed. Daily flood evolution data were extracted and spatialized using ArcGIS 10.5 software to generate a four-day flood inundation map (Figure 3). Additionally, the submerged areas on different dates of the CPEC were identified from the results. The total affected areas were 3.56 million km² on 27 July, rising to 3.58 million km² on 28 July, further increasing to 3.64 million km² on 29 July, then slightly decreasing to 3.61 million km² on 30 July—totaling 14.36 million km².

Furthermore, it is evident from the map that the northern region of the corridor and China's portion of it remained a portion affected by flooding during this event. Severe flooding occurred in Sindh Province due to coastal proximity and flat terrain, with depths reaching 8 m or more. Substantial inundation also occurred at Punjab's river confluences. Flooding in Balochistan was limited to the lower Indus border with Sindh. Overall, severe effects concentrated in the Indus Plain, with less impact in northern CPEC.

The calculated submerged area of the CPEC during the peak period was compared with the actual flood-affected area data for the corridor, as reported by the United Nations Office for the Coordination of Humanitarian Affairs in 2010. As shown in Figure 4, the correlation coefficient between the actual inundation area and the simulated inundation area is 0.734. On the one hand, flood inundation is closely related to flood control facilities and human activities. Human activities in Sindh Province have transformed the microtopography, which is highly disorderly, so it is difficult to carry out scene simulation in the model. On the other hand, the landscape within Sindh consists mainly of alluvial plains on both sides of the Indus River, and due to the low topography of some areas, the difference in elevation between the grids is not significant. This small difference leads to some errors in modeling the inundation analysis, and the inundated area of Sindh in the modeling results deviates from the actual results. Overall, the simulation results demonstrate reasonable consistency with the actual damage situation, thereby facilitating their utilization in subsequent flood risk assessment and analysis.

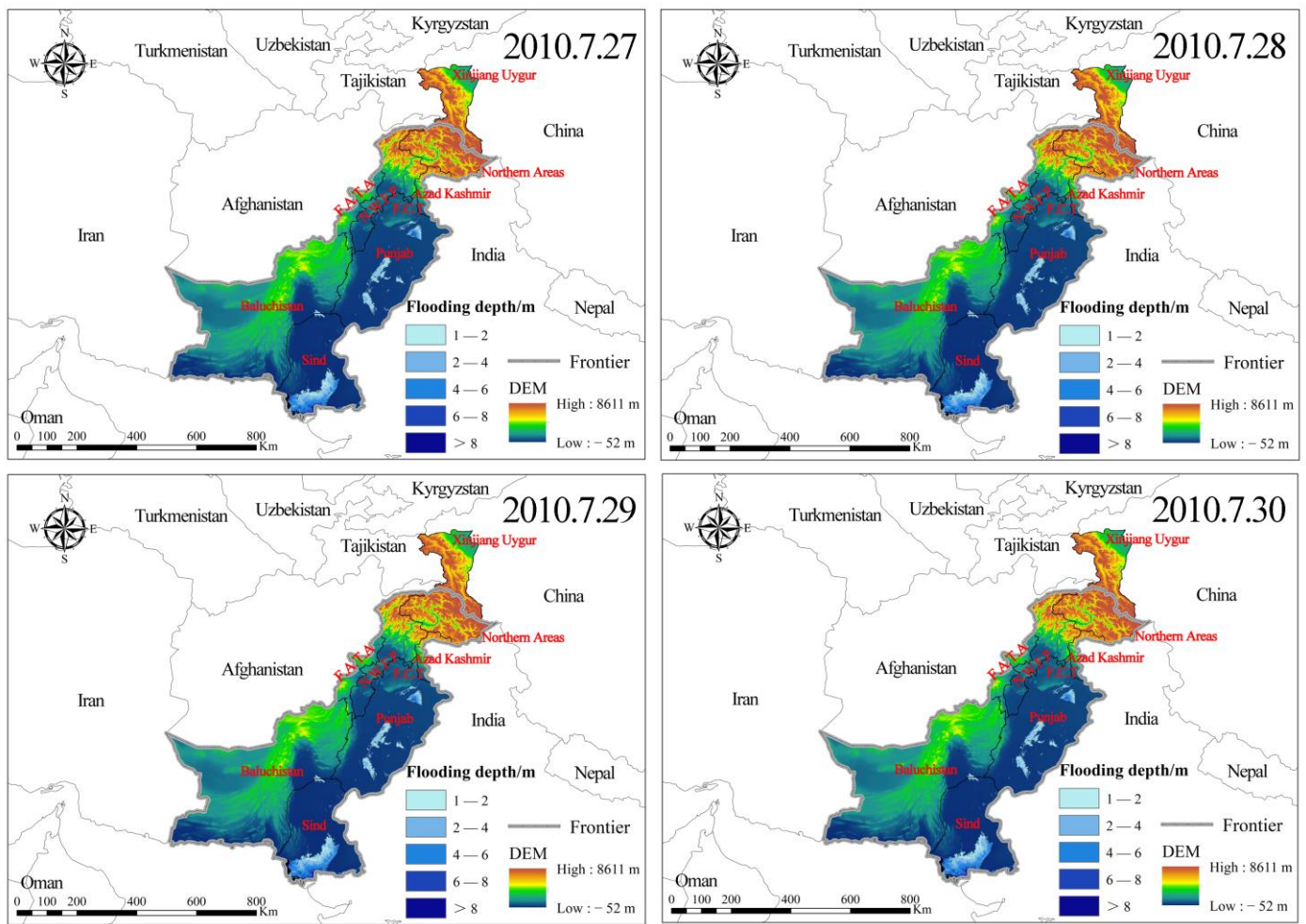


Figure 3. Flooding depths in various areas of the CPEC under a 100-year flood scenario.

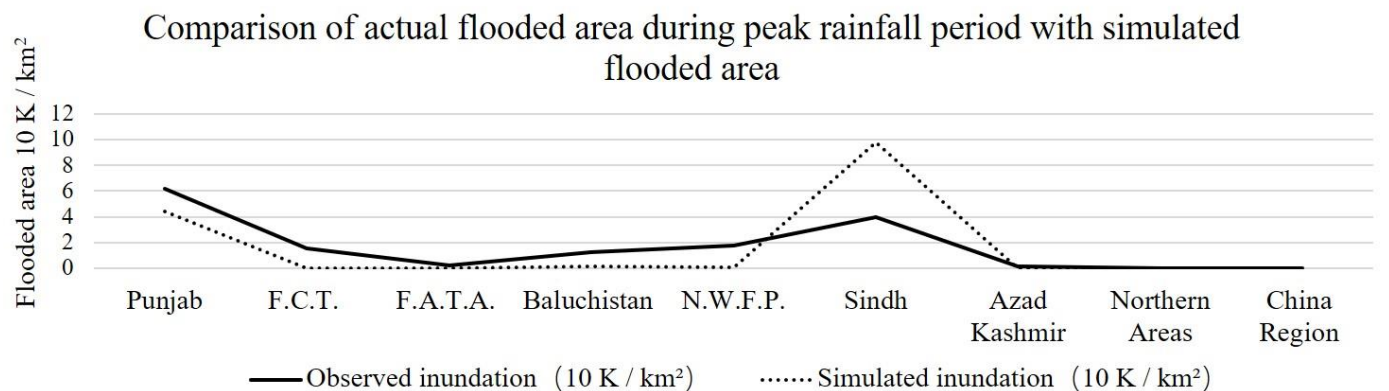


Figure 4. Comparison of the observed flooded area during peak rainfall period with simulated flooded area.

3.3.2. Flood Hazard Assessment

The high-resolution flood depth simulations enabled precise spatial analysis of flood risk variations. By overlaying the four-day peak flood depths (Figure 5) and normalizing the results (Figure 6), the hazard was assessed based solely on inundation depth. Extensive flooding occurred in the flat Punjab and Sindh Provinces, with typical depths of 1–4 m (Figures 5 and 6). However, certain regions, such as Hafizabad (Punjab) and Sindh coastal areas, exceeded 8 m. Intense rainfall also caused 1–2 m flooding along the lower-middle

Indus banks in Balochistan. While minor inundation existed in northern CPEC, dams mitigated large floods. The Punjab Plains face high flood risk overall, but the deepest inundation concentrates in Sindh.

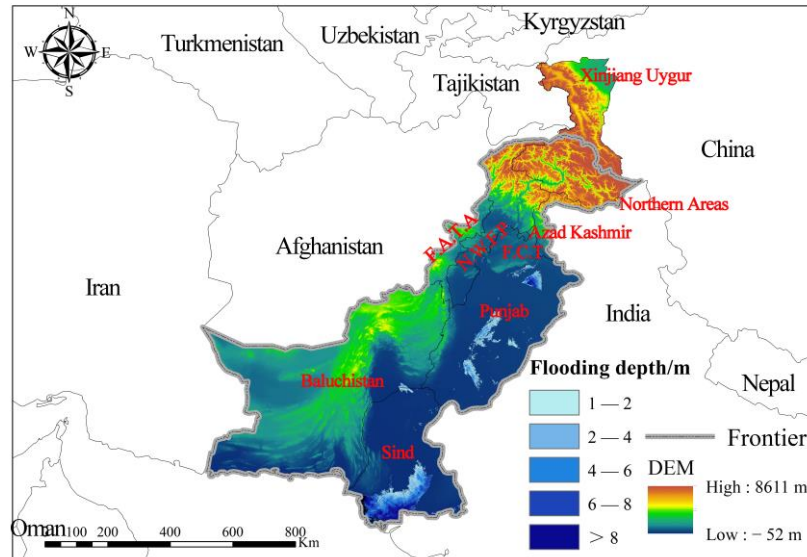


Figure 5. Four-day average flooding depth under a 100-year flood scenario.

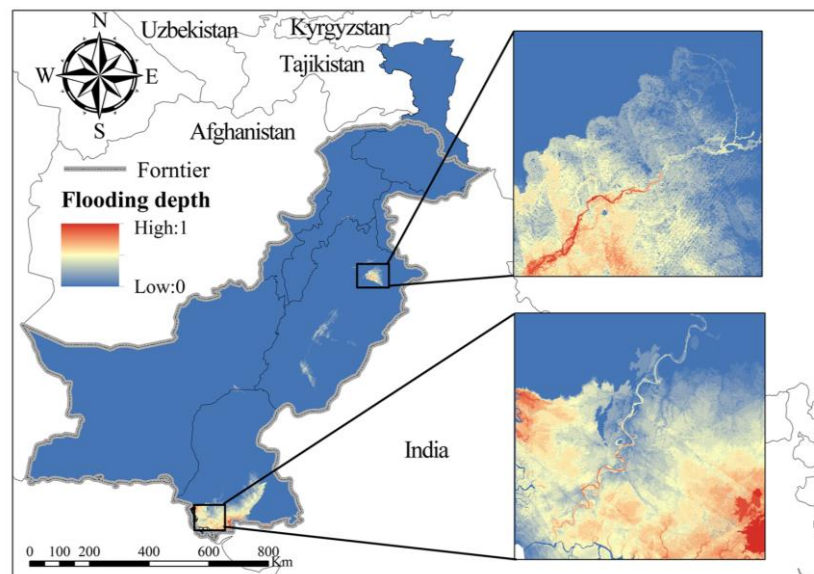


Figure 6. Normalized flood hazard assessment under a 100-year flood scenario.

3.3.3. Flood Vulnerability Assessment

Vulnerability indicators, such as population density, road density, and arable land density, served as positive indicators of flood risk. Grid-based densities were calculated and standardized using ArcGIS Raster Calculator (Figure 7). Analysis revealed socioeconomic development centered along the Indus Basin. Notably, Lahore, Punjab, had the highest road density due to its status as Pakistan’s second-largest city and industrial hub with high infrastructure demands. Currently, roads primarily connect major cities such as Lahore, Karachi, Quetta, and Islamabad. Fewer roads linked China and Pakistan in northern CPEC. As an agricultural country, Pakistan displayed higher arable land density in the Punjab Plains. The fertile alluvial plain of the Indus River extending into Sindh enables substantial cultivation. Conversely, mountainous northern regions had lower farmland

density. Population density aligned with road and arable land patterns. Significant urban–rural differences existed, with megacities such as Lahore, Islamabad, and Karachi having higher densities than northern areas and Balochistan.

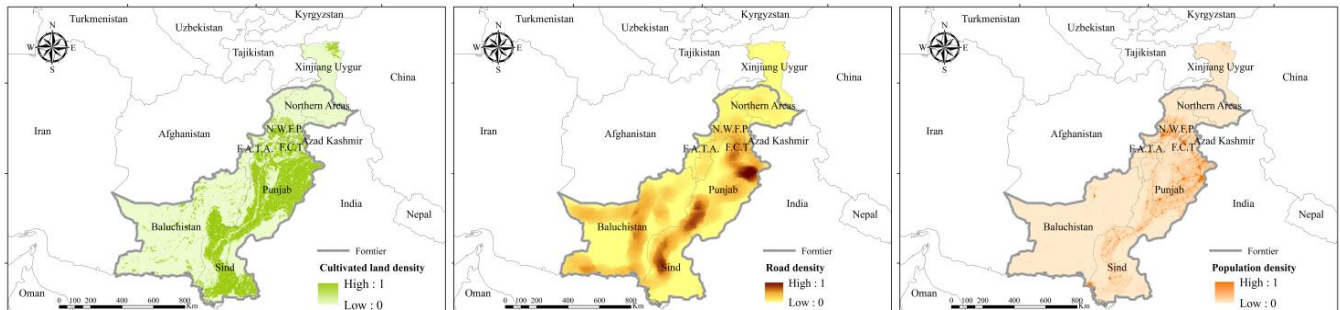


Figure 7. Normalization of vulnerability indicators.

Based on the weighting results, a combination of population density, farmland density, and road was utilized to assess flood vulnerability using the raster calculator. The results are shown in Figure 8. It shows that areas with high vulnerability in the CPEC are mainly concentrated in the Punjab and Sindh Provinces as well as the Federal Capital Territory. Among these regions, the Federal Capital Territory exhibits the highest proportion of vulnerable areas at 57.15%, while Punjab and Sindh have proportions of 48.84% and 26.49%, respectively. In the concept of flood risk assessment, flood risk is a probability. At the present stage, the flood in the study area may not have occurred. What we do is assess the possible future risks in the area. From the disaster system theory, vulnerability refers to the possibility of damage when the carrier system is attacked by natural disasters in a certain social and economic environment. The calculation of vulnerability ratios is carried out by counting the high-risk grids in the administrative districts, and although the Federal Capital Territory is economically developed and highly resilient to disasters, the vulnerability of the area also needs to be considered. What we are doing is an assessment of what the vulnerability might be in the future. Regions such as Federal Capital Territory exhibit elevated population densities, concentrated road networks, and a significant proportion of cropland, rendering them susceptible to substantial socioeconomic losses in case of a flood. The Balochistan Province had predominantly medium-low vulnerability, with some high-risk pockets along roads (4.17% of the total). The northern region (97.73%), FATA (83.02%), and Chinese corridor (91.70%) had mainly low vulnerability due to constrained valley settlements, sparse populations, limited farmland, and underdeveloped infrastructure. These conditions minimize casualties and losses even during major floods.

3.3.4. Flood Sensitivity Assessment

The flood sensitivity index system includes elevation, slope, and NDVI as negative indicators. This implies that as these indicators increase, the risk of floods decreases. In this study, all sensitivity data collected from the CPEC area were normalized for classification purposes. Punjab and Sindh Provinces have lower elevations and slopes, corresponding to higher flood risks. The northern region and junction of the Chinese region with the CPEC area are adjacent to the Karakoram Range, with the highest peak being Qogir Feng at 8569 m, resulting in lower overall flood risk. In the western region of the CPEC, comprising mainly the Balochistan Plateau, there is a high flood risk associated with elevation, while moderate to low flood risk exists in terms of slope. Additionally, higher vegetation coverage is inversely associated with the risk of flood disasters. Therefore, according to Figure 9, the flood risk in the Punjab Plain is lower. Conversely, regions such as Balochistan, the northern region, and the Chinese region of the CPEC area exhibit sparse vegetation cover due to natural factors such as elevation, consequently resulting in an elevated susceptibility to flood disasters.

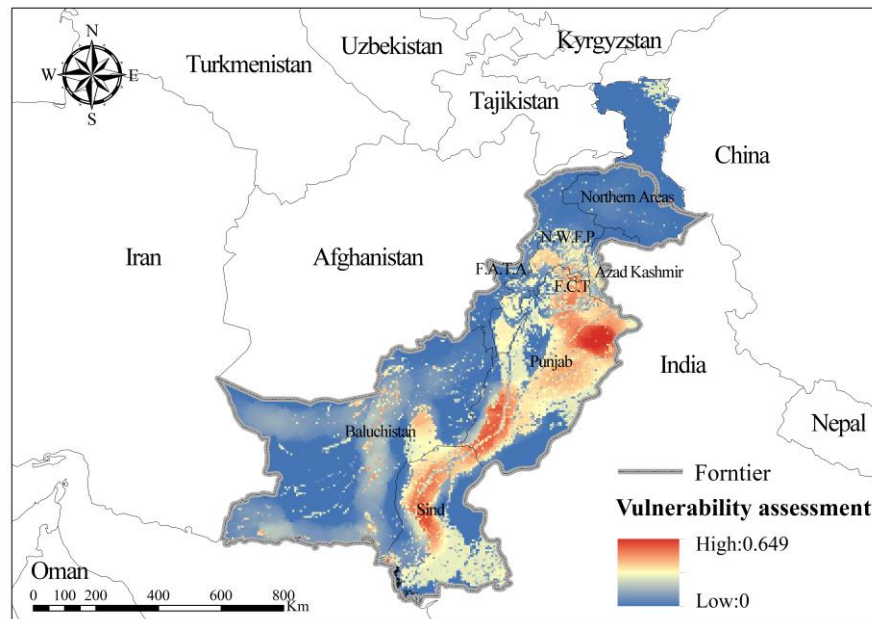


Figure 8. Vulnerability assessment.

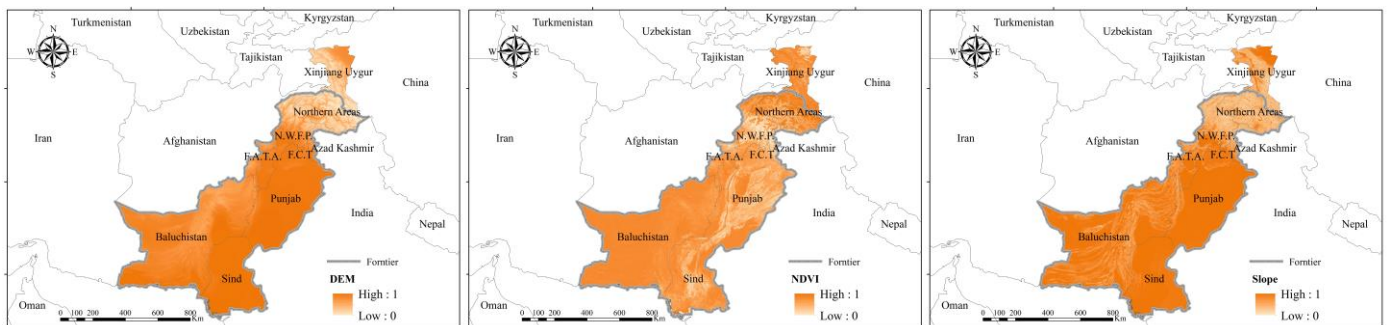


Figure 9. Normalization of sensitivity indicators.

We conducted a sensitivity assessment of floods for the CPEC by integrating elevation, slope, and NDVI with their respective weights. The results are illustrated in Figure 10. They indicate that areas highly susceptible to flooding are primarily concentrated in the Punjab and Sindh Plains and the southwestern region of Balochistan Province. These plain areas exhibit flat terrain, low slopes, and elevations below 500 m, rendering them vulnerable to floods due to the absence of topographic features that can impede floodwaters. Moreover, the desert area in the southwestern part of the Balochistan Province experiences sparse vegetation cover and predominantly lies at an elevation lower than 600 m, making it particularly prone to flooding. Conversely, northern regions and most parts of the Chinese section of the corridor demonstrate low sensitivity levels towards floods, with a minimum sensitivity level recorded at 0.27. This is attributed to their location within the Karakoram Mountains characterized by high elevations and slopes. However, the erosion caused by the Indus River has shaped landforms such as the Hunza Valley, characterized by flat terrain, less than 50% vegetation cover, and a higher risk of flooding compared to other parts of the northern region. Furthermore, the starting point of the CPEC in Kashgar City is located in an alluvial fan plain formed by the Kashgar River system that exhibits high sensitivity. The Balochistan Plateau features north–south parallel mountains with elevations exceeding 3000 m and a broad plateau spanning elevations from 500 to 2000 m. The region experiences a hot and dry climate resulting in sparse vegetation, hence, its sensitivity to flood disasters is classified as medium to high.

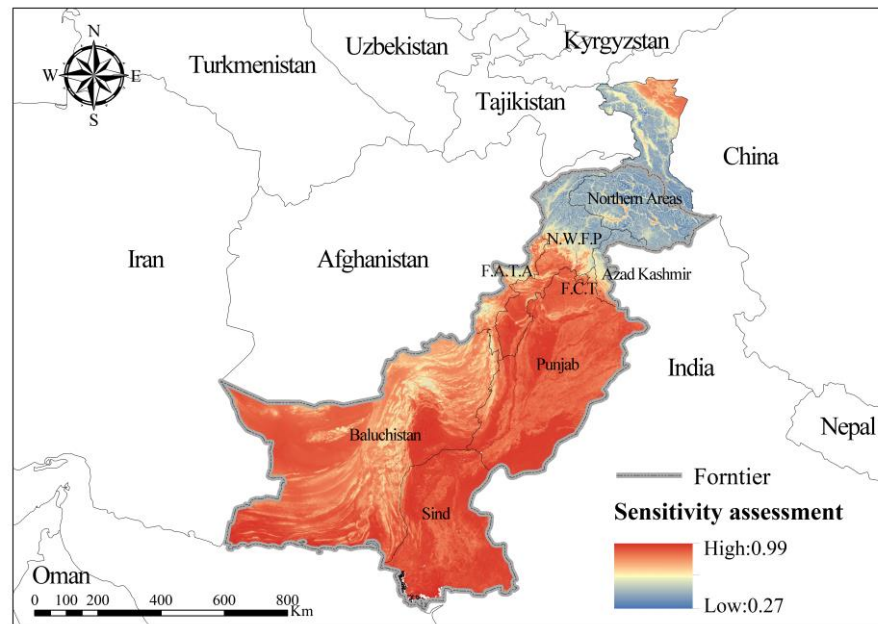


Figure 10. Sensitivity assessment.

3.3.5. Flood Risk Assessment

By superimposing spatial distribution data of hazard, vulnerability, and sensitivity indicators based on their respective weights, we obtained the flood risk assessment results for the typical scenario of the CPEC (Figure 11).

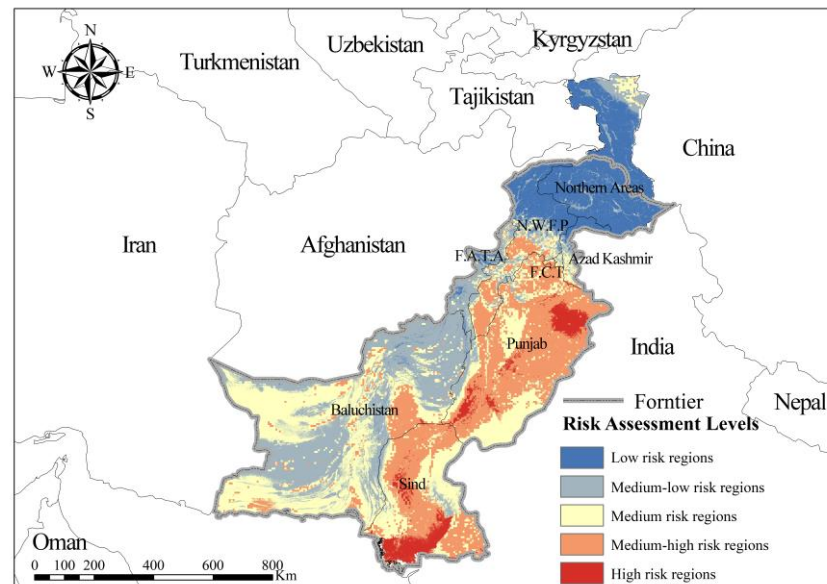


Figure 11. Flood risk assessment.

From a grid cell perspective, the flood risk in the CPEC exhibits an increasing trend from north to south and from west to east. The high-risk areas account for 4.18% of the total area of the corridor, mainly distributed in the eastern and southern parts of Punjab Province and southern and central parts of Sindh Province. These areas are susceptible to flooding during a 100-year flood event due to their proximity to larger cities, which increases their vulnerability and sensitivity to flooding hazards. Medium-high risk encompasses 25.56% of the total area and is mainly concentrated in Punjab and Sindh Provinces, with additional distribution in the Federal Capital Territory, Khyber Pakhtunkhwa Province,

and Balochistan. In total, 54.68% of the total risk area exhibits medium-low and medium risk levels, primarily concentrated in Balochistan with some distribution in Punjab and Sindh. Low-risk areas are more extensively distributed across northern regions and the corridor regions of China, accounting for 15.58% of the total area.

At the regional level, the provinces encompassing all five levels of risk include Azad Kashmir, Balochistan, Khyber Pakhtunkhwa, Punjab and Sindh. In Punjab, areas classified as high-risk account for 8.46% of the total provincial area, medium-high-risk areas constitute 59.74%, medium-risk areas comprise 27.92%, while low- and medium-low-risk areas represent 3.88%. Conversely, in Sindh, a higher percentage of high-risk areas is observed at 15.51%, along with an overall higher proportion of medium-high- and medium-risk areas at 80.01%. Azad Kashmir predominantly consists of low- and medium-low-risk areas covering approximately 66.69% of its territory, with medium-risk zones accounting for 27.56%. In Balochistan, the proportion of low- and medium-low-risk areas is high at 91.09%, and other risk levels are less. Khyber Pakhtunkhwa has a minimal area of high risk at 0.09%, and the proportion of other risk levels is not significantly different. In total, 73.56% of the Corridor China region is categorized as low-risk. FATA consists mainly of medium-low-risk areas, while FCT comprises primarily medium-high-risk areas. The Northern Region is predominantly low-risk at 93.31%, but due to its location in the headwaters of the Indus River, it also contains some medium to low flood-prone regions at 6.69%, without any medium-high risk or high-risk areas.

3.3.6. Validation of the Results

In order to validate our evaluation results, a relevant analytical approach was employed to calculate the correlation coefficient between the simulated results and observed data. First, the frequency of flood events in the various regions of the CPEC between 2001 and 2022 (source: <http://www.adrc.asia>, accessed on 7 December 2023) and the number of people affected by floods in Pakistan in 2010 (source: Pakistan Floods 2010 Report) were selected as the observations. After normalizing the data (Figures 12 and 13), we conducted Pearson correlation analysis based on the grid of the flood risk assessment results. The correlation between the flood risk assessment index and the frequency of flood events was 0.57, while that between the assessment index and the number of people affected by floods was 0.64. Both Punjab and Sindh Provinces exhibited relatively high values for both flood event frequency and number of people affected by floods, whereas the northern region had low values. These findings are consistent with those obtained from our results of the flood risk assessment, thereby lending credibility to our overall evaluation results.

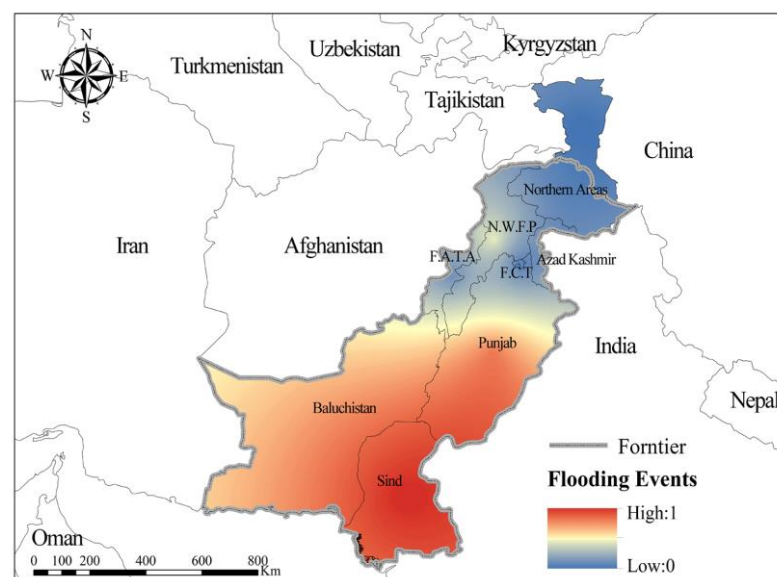


Figure 12. Number of flooding events.

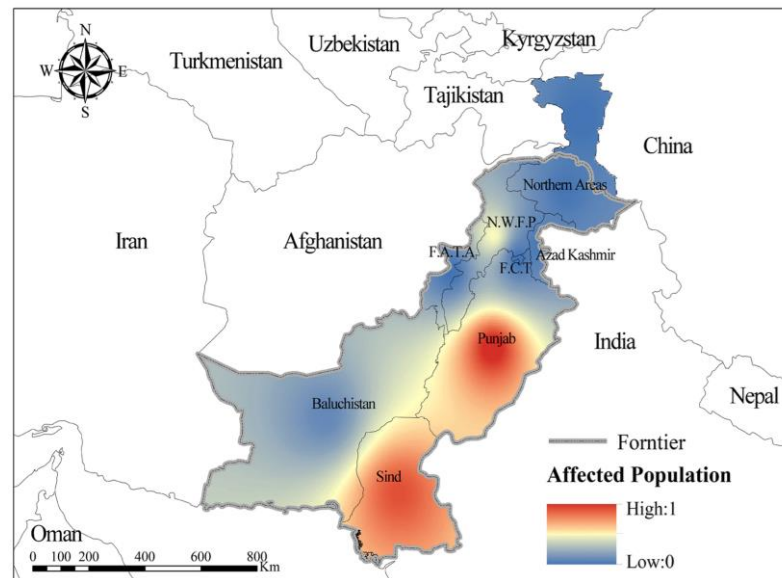


Figure 13. Affected population in 2010.

4. Discussion

Pakistan, which constitutes the primary segment of the CPEC, is among the countries most susceptible to flood disasters. It experiences a high frequency of flood occurrences during the summer season due to extreme rainfall and glacial meltwater. Over the past two decades, Pakistan endured 54 flood disasters of varying intensities, resulting in significant socioeconomic losses. As a result, it ranks 10th in the Global Environmental Risk Index [35]. The northern region of the CPEC has witnessed a substantial rise in temperatures due to global warming [36], leading to increased glacial meltwater. This has particularly heightened the vulnerability to flooding in the Punjab Plains, where Indus tributaries converge, and in Northern Sindh [37]. Moreover, the confluence of the Jhelum River and the Indus River, where water flow reaches its maximum capacity, is exacerbated by the low-lying terrain, rendering it highly vulnerable to flood impacts [38]. During the summer monsoon season, elevated sea surface temperatures in proximity to the Arabian Sea trigger intense convective weather patterns and abundant rainfall along coastal areas, thereby affecting cities such as Karachi in the southern coastal region of Sindh Province. Consequently, this gives rise to devastating flood disasters within these areas [39]. With the exception of Punjab and Sindh Provinces, areas of medium-high risk, such as Balochistan and Khyber Pakhtunkhwa Provinces, also warrant attention. In 2022, severe flooding occurred in both provinces, with continuous extreme rainfall leading to the formation of massive lakes in Balochistan's densely populated right bank of the Indus River [40]. Rivers of Khyber Pakhtunkhwa Province have diminished capacity to withstand floods due to deforestation, encroachment on floodplains, and sedimentation of riverbeds. Consequently, they are highly vulnerable to catastrophic flooding during periods of extreme rainfall [41]. It is worth noting that the Federal Capital Territory (FCT) experiences hill torrents flowing due to localized topography. We are unable to take all tributaries into account when modeling and risk assessment of flood processes in large basins, which makes it impossible to take into account all microbasins. Flood risk is the result of a combination of vulnerability, sensitivity and hazard. In the vulnerability assessment process, the FCT was found to be highly vulnerable due to its high population density, road density, and arable land density. And, due to the topographical features of the area, the FCT is also considered highly sensitive in the sensitivity assessment. Therefore, in addition to flooding, the high sensitivity and vulnerability results in a potentially medium to high flood risk for the area.

Several studies have been conducted on flood risk assessment in the CPEC. For example, Duan et al. (2022) used a triangular fuzzy number hierarchical analysis and support vector machine model to assess flood vulnerability along the Belt and Road,

highlighting the high-vulnerability areas concentrated in the Indus Basin of Pakistan [42]. The National Disaster Management Authority (NDMA) report identified Sindh, Punjab and Balochistan as flood-prone areas. Atif et al. used MODIS data to map the distribution of floods in Pakistan since 2000 and concluded that the central plains and Southeastern Sindh had suffered the most severe floods over the last 21 years [43]. In addition to this, Hussain et al. (2023) created a comprehensive database of natural hazards in Pakistan at the district level and a multi-hazard zoning map, indicating that the majority of flood-prone areas are located in Sindh and South Punjab Provinces [44]. Sajjad et al. (2020) stated that the Chenab Plain is one of the high flood-prone areas with using remote sensing to estimate the extent and duration of flood inundation in Pakistan [45]. In addition, the floods also occurred near the Jhelum River Basin in 2014. It is known from the 2014 Pakistan's flood report that the flood-affected areas were located in the northern, eastern and central parts of Punjab (Lahore, Gujranwala, Rawalpindi and Faisalabad, Sargodha and Multan Provinces). These findings align with the results from flood risk assessments, emphasizing the urgent need for region-specific policy measures to address high-risk floods in the CPEC area, mitigate losses inflicted by flood disasters, and ensure the uninterrupted operation of the corridor.

At present, the Pakistani government has formulated flood prevention plans and warning systems. However, these efforts primarily focus on relief rather than disaster preparedness. Due to the country's unique circumstances, the existing warning system has limited coverage, and local governments have low implementation capabilities for flood prevention policies. The eastern and southern parts of Punjab Province are important waterway nodes for the CPEC, and are the main agricultural planting areas in Pakistan. Therefore, it is necessary to closely monitor river water level changes in this area during the summer and take timely precautions. Moreover, it is advisable to consider increasing flood control infrastructure and implementing appropriate vegetation rehabilitation measures. Sindh Province, located in the middle and lower reaches of the Indus River, faces riverbed siltation that leads to elevated riverbeds. To address this issue, it is necessary to reinforce barrages in the region, increase their storage capacity, and implement effective management strategies. In regions with moderate to high flood risk, precipitation warnings should be intensified, and preparations should be made for the timely evacuation. The multifaceted process of flooding in the CPEC area, driven by global climate change, necessitates a more dynamic approach to flood risk assessments. While current methods rely on remote sensing imagery and socioeconomic statistical data, hydraulic models can provide real-time and fine-grained flood simulations, greatly improving precision and applicability for corridor construction. However, future assessments must integrate multiple influencing factors, including water management infrastructure within the watershed.

5. Conclusions

Floods pose a severe natural disaster risk that needs to be addressed by the China–Pakistan Economic Corridor (CPEC) during its development. Utilizing the MIKE11 hydraulic model to simulate and calculate flood depths in an extreme centennial flood scenario and factoring in socioeconomic and geographical variables, a comprehensive flood risk assessment was conducted using the Analytic Hierarchy Process (AHP) and Entropy Weight Method. The results are as follows:

- (1) The hydraulic model, constructed using data on river cross sections and flow rates, has successfully passed verification tests against observed data with a high evaluation metric (Nash efficiency of 0.861) during the validation period. This good performance demonstrated that the model accurately reflects the water surface status in the study area's rivers, providing a solid foundation for the calculation of flood water depths.
- (2) The flood depth map reveals that the floods are mainly concentrated in the relatively flat provinces of Punjab and Sindh, with depths mostly ranging from 1 to 4 m. However, in the Hafizabad area of Punjab and the coastal areas of Sindh, the flood depths are relatively higher, exceeding 8 m. Floods also occurred in Balochistan, with depths

ranging from 1 to 2 m. The simulated results agreed well with the observed flood data in Pakistan in 2010, with an overall correlation coefficient of 0.734, attesting to the consistency between the two datasets and endorsing their application for future flood risk assessments and analysis.

- (3) The flood disaster risk in the CPEC exhibits an increasing trend from the north to the south and from the west to the east, with high-risk areas accounting for 4.18% of the total area. These areas are mainly distributed in the eastern part of Punjab Province, the southern part of Sindh Province, the confluence zones of rivers in Punjab Province, and the central part of Sindh Province. The medium-high-risk areas cover 25.56% of the total area, concentrated in Punjab and Sindh Provinces, with scattered occurrences in the Federal Capital Territory, Khyber Pakhtunkhwa Province, and the Balochistan Province. The medium- and medium-low-risk areas cover 54.68% of the total area, mainly concentrated in Balochistan Province. Meanwhile, low-risk areas cover 15.58% of the total area and are widely distributed across the northern regions and the Chinese corridor region. These assessment results align closely with the observed disaster damage data, providing robust empirical support for flood prevention and disaster relief efforts within the CPEC region.

Author Contributions: All authors wrote the main manuscript text. X.S. and K.J. applied the model. H.T. and Z.D. analyzed the data. X.S. and C.G. prepared Figures. All authors reviewed the manuscript. All authors have read and agreed to the published version of the manuscript.

Funding: This research received no external funding.

Data Availability Statement: The data used to substantiate the findings of this research are accessible upon request from the corresponding author.

Conflicts of Interest: The authors declare no conflict of interest.

References

1. Wang, X.X.; Jiang, D.B.; Lang, X.M. Future extreme climate changes linked to global warming intensity. *Sci. Bull.* **2017**, *62*, 1673–1680. [[CrossRef](#)] [[PubMed](#)]
2. Mateo-Garcia, G.; Veitch-Michaelis, J.; Smith, L.; Oprea, S.V.; Schumann, G.; Gal, Y.; Baydin, A.G.; Backes, D. Towards global flood mapping onboard low cost satellites with machine learning. *Sci. Rep.* **2021**, *11*, 7249. [[CrossRef](#)]
3. Khan, B.; Iqbal, M.J.; Yosufzai, M.A.K. Flood risk assessment of River Indus of Pakistan. *Arab. J. Geosci.* **2011**, *4*, 115–122. [[CrossRef](#)]
4. Cai, S.Y.; Fan, J.M.; Yang, W. Flooding Risk Assessment and Analysis Based on GIS and the TFN-AHP Method: A Case Study of Chongqing, China. *Atmosphere* **2021**, *12*, 623. [[CrossRef](#)]
5. Bin, L.L.; Xu, K.; Pan, H.; Zhuang, Y.C.; Shen, R.Z. Urban flood risk assessment characterizing the relationship among hazard, exposure, and vulnerability. *Environ. Sci. Pollut. Res.* **2023**, *30*, 86463–86477. [[CrossRef](#)]
6. Peng, J.Q.; Zhang, J.M. Urban flooding risk assessment based on GIS- game theory combination weight: A case study of Zhengzhou City. *Int. J. Disaster Risk Reduct.* **2022**, *77*, 103080. [[CrossRef](#)]
7. Aronica, G.T.; Candela, A.; Fabio, P.; Santoro, M. Estimation of flood inundation probabilities using global hazard indexes based on hydrodynamic variables. *Phys. Chem. Earth* **2012**, *42–44*, 119–129. [[CrossRef](#)]
8. Li, X.W.; Du, J.G.; Long, H.Y.; Sun, G.L. Characteristics and risk analysis of hydrological disaster events from 1949 to 2015 in Urumqi, China. *Theor. Appl. Climatol.* **2019**, *137*, 745–754. [[CrossRef](#)]
9. Benito, G.; Lang, M.; Barriendos, M.; Llasat, M.C.; Frances, F.; Ouarda, T.; Thorndycraft, V.R.; Enzel, Y.; Bardossy, A.; Coeur, D.; et al. Use of systematic, palaeoflood and historical data for the improvement of flood risk estimation. review of scientific methods. *Nat. Hazards* **2004**, *31*, 623–643.
10. Anees, M.T.; Abdullah, K.; Nawawi, M.N.M.; Rahman, N.N.N.A.; Piah, A.R.M.; Zakaria, N.A.; Syakir, M.I.; Omar, A.K.M. Geological Society of Africa Presidential Review Numerical modeling techniques for flood analysis. *J. Afr. Earth Sci.* **2016**, *124*, 478–486. [[CrossRef](#)]
11. Taraky, Y.M.; Liu, Y.B.; McBean, E.; Daggupati, P.; Gharabaghi, B. Flood Risk Management with Transboundary Conflict and Cooperation Dynamics in the Kabul River Basin. *Water* **2021**, *13*, 1513. [[CrossRef](#)]
12. Santos, P.P.; Pereira, S.; Zezere, J.L.; Tavares, A.O.; Reis, E.; Garcia, R.A.C.; Oliveira, S.C. A comprehensive approach to understanding flood risk drivers at the municipal level. *J. Environ. Manag.* **2020**, *260*, 110127. [[CrossRef](#)] [[PubMed](#)]
13. Zhao, Y.J.; Wang, H.; Liu, Z.L.; Wu, S.; Ma, Q.Q. Multi-scenario waterlogging disaster risk assessment based on combination weighting. *Water Resour. Hydropower Eng.* **2022**, *53*, 1–12. (In Chinese) [[CrossRef](#)]

14. Zhang, W.T.; Liu, Y.Z.; Tang, W.W.; Wang, W.; Liu, Z. Assessment of the effects of natural and anthropogenic drivers on extreme flood events in coastal regions. *Stoch. Environ. Res. Risk Assess.* **2023**, *37*, 697–715. [[CrossRef](#)]
15. Hartmann, H.; Buchanan, H. Trends in Extreme Precipitation Events in the Indus River Basin and Flooding in Pakistan. *Atmos. Ocean* **2014**, *52*, 77–91. [[CrossRef](#)]
16. Houze, R.A.; Rasmussen, K.L.; Medina, S.; Brodzik, S.R.; Romatschke, U. Anomalous Atmospheric Events Leading to the Summer 2010 Floods in Pakistan. *Bull. Am. Meteorol. Soc.* **2011**, *92*, 291–298. [[CrossRef](#)]
17. Iqbal, A.; Hassan, S.A. ENSO and IOD analysis on the occurrence of floods in Pakistan. *Nat. Hazards* **2018**, *91*, 879–890. [[CrossRef](#)]
18. Nanditha, J.S.; Kushwaha, A.P.; Singh, R.; Malik, I.; Solanki, H.; Chuphal, D.S.; Dangar, S.; Mahto, S.S.; Vegad, U.; Mishra, V. The Pakistan Flood of August 2022: Causes and Implications. *Earths Future* **2023**, *11*, e2022EF003230. [[CrossRef](#)]
19. Viterbo, F.; von Hardenberg, J.; Provenzale, A.; Molini, L.; Parodi, A.; Sy, O.O.; Tanelli, S. High-Resolution Simulations of the 2010 Pakistan Flood Event: Sensitivity to Parameterizations and Initialization Time. *J. Hydrometeorol.* **2016**, *17*, 1147–1167. [[CrossRef](#)]
20. Webster, P.J.; Toma, V.E.; Kim, H.M. Were the 2010 Pakistan floods predictable? *Geophys. Res. Lett.* **2011**, *38*, L04806. [[CrossRef](#)]
21. Charles, S.P.; Wang, Q.J.; Ahmad, M.U.D.; Hashmi, D.; Schepen, A.; Podger, G.; Robertson, D.E. Seasonal streamflow forecasting in the upper Indus Basin of Pakistan: An assessment of methods. *Hydrol. Earth Syst. Sci.* **2018**, *22*, 3533–3549. [[CrossRef](#)]
22. Ma, Y.Y.; Hu, X.X.; Chen, Y.T.; Hu, Z.Y.; Feng, T.C.; Feng, G.L. Different Characteristics and Drivers of the Extraordinary Pakistan Rainfall in July and August 2022. *Remote Sens.* **2023**, *15*, 2311. [[CrossRef](#)]
23. Khan, I.; Lei, H.D.; Shah, A.A.; Khan, I.; Muhammad, I. Climate change impact assessment, flood management, and mitigation strategies in Pakistan for sustainable future. *Environ. Sci. Pollut. Res.* **2021**, *28*, 29720–29731. [[CrossRef](#)] [[PubMed](#)]
24. Vojinovic, Z.; Seyoum, S.D.; Mwalwaka, J.M.; Price, R.K. Effects of model schematisation, geometry and parameter values on urban flood modelling. *Water Sci. Technol.* **2011**, *63*, 462–467. [[CrossRef](#)]
25. Timbe, L.M.; Timbe, E.P. Mapeo del peligro de inundación en ríos de montaña, caso de estudio del río Burgay. *Maskana* **2012**, *3*, 87–96. [[CrossRef](#)]
26. Di Baldassarre, G.; Schumann, G.; Bates, P.D.; Freer, J.E.; Beven, K.J. Flood-plain mapping: A critical discussion of deterministic and probabilistic approaches. *Hydrol. Sci. J.* **2010**, *55*, 364–376. [[CrossRef](#)]
27. Timbe, L.; Willems, P. Desempeño de modelos hidráulicos 1D y 2D para la simulación de inundaciones. *Maskana* **2011**, *2*, 91–98. [[CrossRef](#)]
28. Ali, A.M.; Solomatine, D.P.; Di Baldassarre, G. Assessing the impact of different sources of topographic data on 1-D hydraulic modelling of floods. *Hydrol. Earth Syst. Sci.* **2015**, *19*, 631–643. [[CrossRef](#)]
29. Vojtek, M.; Vojteková, J. 2016 Flood hazard and flood risk assessment at the local spatial scale: A case study. *Geomat. Nat. Hazards Risk.* **2016**, *7*, 1973–1992. [[CrossRef](#)]
30. Danish Hydraulic Institute (DHI). *MIKE 11: A Modeling System for Rivers and Channels Reference Manual*; Danish Hydraulic Institute (DHI): Hørsholm, Denmark, 2005.
31. Li, G.; Li, J.P.; Sun, X.L.; Zhao, M. Research on a Combined Method of Subjective-Objective Weighing and the its Rationality. *J. Manag. Rev.* **2017**, *29*, 17–26+61. (In Chinese) [[CrossRef](#)]
32. Saaty, T.L. How to make a decision: The analytic hierarchy process. *Eur. J. Oper. Res.* **1990**, *48*, 9–26. [[CrossRef](#)]
33. Wu, J.; Chen, X.; Lu, J. Assessment of long and short-term flood risk using the multi-criteria analysis model with the AHP-Entropy method in Poyang Lake basin. *Int. J. Disaster Risk Reduct.* **2022**, *75*, 102968. [[CrossRef](#)]
34. He, H.; Zhou, J.; Zhang, W. Modelling the impacts of environmental changes on hydrological regimes in the Hei River Watershed, China. *Glob. Planet Change* **2008**, *61*, 175–193. [[CrossRef](#)]
35. Manzoor, Z.; Ehsan, M.; Khan, M.B.; Manzoor, A.; Akhter, M.M.; Sohail, M.T.; Hussain, A.; Shafi, A.; Abu-Alam, T.; Abioui, M. Floods and flood management and its socio-economic impact on Pakistan: A review of the empirical literature. *Front. Environ. Sci.* **2022**, *10*, 2480. [[CrossRef](#)]
36. Yu, Z.X.; Yu, X.J.; Yang, F. Spatio-temporal characteristics of climate change in China-Pakistan Economic Corridor from 1980 to 2019. *J. Arid Zone Res.* **2021**, *38*, 695–703. (In Chinese) [[CrossRef](#)]
37. Ali, S.M.; Khalid, B.; Akhter, A.; Islam, A.; Adnan, S. Analyzing the occurrence of floods and droughts in connection with climate change in Punjab province, Pakistan. *Nat. Hazards* **2020**, *103*, 2533–2559. [[CrossRef](#)]
38. Shahid, H.; Toyoda, M.; Kato, S. Impact Assessment of Changing Landcover on Flood Risk in the Indus River Basin Using the Rainfall-Runoff-Inundation (RRI). *Sustainability* **2022**, *14*, 7021. [[CrossRef](#)]
39. Paulikas, M.J.; Rahman, M.K. A temporal assessment of flooding fatalities in Pakistan (1950–2012). *J. Flood Risk Manag.* **2015**, *8*, 62–70. [[CrossRef](#)]
40. Nazeer, M.; Bork, H. A local scale flood vulnerability assessment in the flood-prone area of Khyber Pakhtunkhwa, Pakistan. *Nat. Hazards* **2022**, *111*, 1103. [[CrossRef](#)]
41. Atta-ur-Rahman; Khan, A.N. Analysis of 2010-flood causes, nature and magnitude in the Khyber Pakhtunkhwa, Pakistan. *Nat. Hazards* **2013**, *66*, 887–904. [[CrossRef](#)]
42. Duan, Y.; Xiong, J.N.; Cheng, W.M.; Wang, N.; Li, Y.; He, Y.F.; Liu, J.; He, W.; Yang, G. Flood vulnerability assessment using the triangular fuzzy number-based analytic hierarchy process and support vector machine model for the Belt and Road region. *Nat. Hazards* **2022**, *110*, 269–294. [[CrossRef](#)]
43. Atif, S.; Umar, M.; Ullah, F. Investigating the flood damages in Lower Indus Basin since 2000: Spatiotemporal analyses of the major flood events. *Nat. Hazards* **2021**, *108*, 2357–2383. [[CrossRef](#)]

44. Hussain, M.A.; Zhang, S.; Muneer, M.; Moawwez, M.A.; Kamran, M.; Ahmed, E. Assessing and Mapping Spatial Variation Characteristics of Natural Hazards in Pakistan. *Land* **2023**, *12*, 140. [[CrossRef](#)]
45. Sajjad, A.; Lu, J.; Chen, X.; Chisenga, C.; Saleem, N.; Hassan, H. Operational Monitoring and Damage Assessment of Riverine Flood-2014 in the Lower Chenab Plain, Punjab, Pakistan, Using Remote Sensing and GIS Techniques. *Remote Sens.* **2020**, *12*, 714. [[CrossRef](#)]

Disclaimer/Publisher's Note: The statements, opinions and data contained in all publications are solely those of the individual author(s) and contributor(s) and not of MDPI and/or the editor(s). MDPI and/or the editor(s) disclaim responsibility for any injury to people or property resulting from any ideas, methods, instructions or products referred to in the content.